Electronic Spectroscopy of Biphenylene Inside Helium Nanodroplets[†]

Özgür Birer,[‡] Paolo Moreschini,[‡] Kevin K. Lehmann,*[,§] and Giacinto Scoles[‡,||]

Chemistry Department, Princeton University, Princeton, New Jersey 08544, Chemistry Department, University of Virginia, Charlottesville, Virginia 22903, and Scuola Internazionale Superiore Di Studi Avanzati, Via Beirut 2-4, Trieste 34014, Italy

Received: January 28, 2007; In Final Form: April 2, 2007

We have recorded the $S_1 \leftarrow S_0$ electronic spectra of Biphenylene and its Ar and O_2 van der Waals complexes inside helium nanodroplets using beam depletion detection. In general, the spectrum is similar to the previously reported high-resolution REMPI spectrum. The zero phonon lines, however, are split similar to the previously reported tetracene case. The calculated potential energy surface predicts that helium atoms can simultaneously occupy all equivalent global minima positions. Therefore, it appears that the splitting cannot be explained either by different isomers or by tunneling. Furthermore, surprisingly the splitting is retained for the Ar van der Waals complexes (and possibly for the O_2 complex as well). This case suggests that the current models of the origin of zero phonon line splitting and the helium solvation are incomplete.

1. Introduction

Solvation of polycyclic aromatic molecules inside helium nanodroplets has drawn attention in the recent years.[1-3] Although it is generally accepted that the observed lineshapes in the electronic spectra are closely related to the details of the solvation, the specifics are still far from understood—we are not yet able to predict even the qualitative features of a spectrum. The $S_1 \leftarrow S_0$ electronic spectra of benzene,[4,5] substituted benzenes,[5] naphthalene,[6] anthracene,[7] tetracene,[8-12] pentacene,[8,11,12] PTCDA,[13,14] porphyrin,[11] phthalocyanines,[11,15-17] perylene,[12,18] benzo[b]fluorene,[19] and the $S_2 \leftarrow S_0$ spectrum of pyrene[20] have been recorded using beam depletion, laser induced fluorescence and/or dispersed emission detection. Van der Waals complexes of benzene, tetracene and pentacene with Ar inside helium droplets have been studied.[4,8] A "typical" spectral line shape is composed of a sharp (~ 1 cm^{-1} fwhm) zero phonon line (ZPL) and a weak phonon wing extending several cm^{-1} to the blue. The ZPL represents excitation of only the chromophore, whereas the phonon wing includes an excitation of helium solvation density (phonons). Usually, there is a gap about 5–6 cm^{-1} between the ZPL and the maximum of the phonon wing, which was interpreted as the first experimental proof of superfluidity of the helium droplets (i.e., the roton maximum in the density of states).[21] However, there are several anomalous cases. For instance, tetracene has a splitting observed for each zero phonon line whereas pentacene does not. Complexation of tetracene with a single argon atom quenches the ZPL splitting for the dominant isomer of the complex.[8,9] The tetracene–helium interaction potential showed that the interaction was strongest for a helium atom over either of the two inner rings. These binding sites cannot be occupied by distinct helium atoms at the same time on the same side of the molecule due to the short distance between them.[9] Therefore, the origin of the ZPL splitting was attributed to two possible sources. The first

possibility is that there are different isomers arising from different localizations of helium atoms over these ring positions, i.e., two helium atoms localized on opposite sides of the same ring or on different rings on opposite sides of the molecule.[9] The second possibility is the tunneling of a single helium atom back and forth between these two minima positions.[9] An extension of this idea involves the simultaneous tunneling of two helium atoms on different sides of the molecule but in opposite directions.[9] Whereas for tetracene and pentacene the zero phonon lines are fully resolved and a distinct gap between the ZPL(s) and the phonon wing is observed, anthracene shows partially resolved split ZPLs and a phonon wing that starts immediately after the ZPLs.[7] This unexpected band structure was attributed to possible combination bands involving the vibrational excitation of the nearest shell of He atoms. Recent time-resolved density functional calculations predict that even with an isotropic potential, some phonon states localized in the first solvation shell can become "soft", even becoming unstable as the interaction is strengthened.[22]

In this study, we present the S_1 ($^1B_{3g}$) $\leftarrow S_0$ electronic spectra of Biphenylene (BP) inside helium nanodroplets (HENDI). Due to its peculiar photophysical properties, BP has been studied extensively both experimentally and theoretically.[23-25] This forbidden electronic transition has a molecular extinction coefficient $\epsilon \approx 150$ M^{-1} cm^{-1}.[23] Normal modes with b_{2u} symmetry enable Herzberg–Teller allowed vibronic transitions by coupling to the allowed S_2 state of B_{1u} symmetry. Experimental studies carried out in vapor and solution phases have limited resolution due to congestion. The first analysis based on high-resolution vapor spectrum was presented by Zanon.[23] The molecule has an extremely low fluorescence quantum yield, on the order of 10^{-4}, and the excited-state lifetime is about 250 ps.[26] The short lifetime was attributed to a large Franck–Condon overlap factor, which is due to a large geometry change.[26]

The only high-resolution electronic spectrum of jet cooled Biphenylene was taken with two color resonance enhanced multiphoton ionization (REMPI) technique by Zimmermann.[27] (Zimmermann inverted the *x* and *z* axes and thus changed the

Biphenylene Inside Helium Nanodroplets

J. Phys. Chem. A, Vol. 111, No. 31, 2007 **7625**

symmetry labels.) The observed vibronic progressions in the S_1 manifold belong to a_g symmetry modes, riding on false origins of b_{2u} symmetry. Although Zimmerman did not provide a quantitative analysis for peak intensities, Marconi calculated vibronic and Franck−Condon terms[28] and compared them to glass matrix spectra taken by Hertzberg and Nickel.[24,25] A simplified calculation for peak intensities will be presented here.

2. Experimental Section

The experiments were carried out on the Princeton droplet spectrometer, which was described in detail previously.[29] Briefly, the spectrometer consists of two differentially pumped chambers evacuated by oil diffusion pumps. The source chamber has a 10-micrometer nozzle, which is cooled down to 17 K by closed cycle refrigerators. Ultrapure (99.9999%) helium gas under 750 psi (50 Bar) pressure is expanded into vacuum to form clusters with an average size of ∼6500 atoms/droplet.[30] The beam passes a 390 μm skimmer, about 1 cm downstream, as it enters the detection chamber. In this chamber, there are 3 pickup cells, which are used to dope the droplets with the species under study. Two of the pickup cells are ovens, the third one is for gaseous or high vapor pressure liquid species. BP (99%, Aldrich) is loaded into one of the ovens and heated (∼45−60 °C) until its vapor pressure is around 10^{-4} Torr. The doped droplets interact with the laser in a multipass cell, which is composed of two flat high reflector mirrors separated by spacers with a wedge. The wedge causes, with proper alignment, the laser beam to exit the vacuum chamber at the location it first enters, after passing the molecular beam approximately 30 times. The detector is an optothermal bolometer,[31] which monitors the flux of the droplet beam. The bolometer has a specified noise equivalent power of 0.13 pW/$\sqrt{\text{Hz}}$, which translates to about 100 nV of noise under experimental conditions, which can be compared to a chopped beam intensity of ∼13 mV. Because BP is a nonfluorescent molecule, when it relaxes from the excited-state, it deposits all of excitation energy into the droplet causing evaporation and shrinking in size. The bolometer detects the depletion in beam flux when the laser is on resonance with an electronic transition. The bolometer signal was amplified first by a cold J230 JFET,[31] then by a Stanford SR550 preamplifier, and finally demodulated by a Stanford SR510 lock-in amplifier.

The laser was a frequency doubled $Ti:Al_2O_3$ setup, which is a modified Indigo[32] system running with the Littman cavity[33] design. The Indigo is pumped by an Evolution-30,[32] a diode pumped intra-cavity frequency doubled Nd:YLF laser. An angle-tuned LBO crystal generates the second harmonic of the laser light. The laser cavity and the LBO crystal are tuned by stepper motor driven mounts, which were added to the system. The laser can scan about 2000 cm^{-1} in the second harmonic region with a bandwidth less than 0.2 cm^{-1}. The average pulse energy was about 150 μJ, and the pulse width was ∼10 ns. The laser fundamental wavelength was monitored by a Burleigh WA-4500 wavemeter.[34] The frequency calibration was achieved with a 7 cm^{-1} free spectral range Etalon and a Ni−Ne hollow cathode optogalvanic lamp. The laser repetition rate was 1 kHz, but due to the limited frequency response of the bolometer, we modulated the light intensity at 250 Hz with a reflective chopper. The reflected pulses were used to monitor the power of the laser during scanning. The control of the laser system and data acquisition were performed with a PC running a custom program written in Labview.[35]

Normal modes were calculated at B3LYP and RHF levels in the ground state and at RCIS level in the first excited-state with a 6-311+G(d, p) basis set. The oscillator strength of the
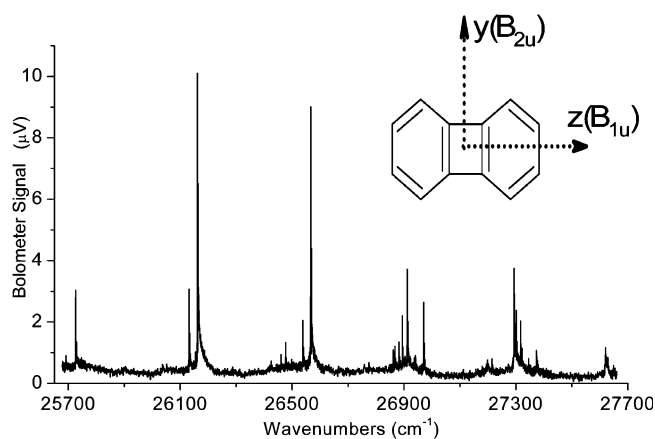

Figure 1. S_1−S_0 transition spectrum of Biphenylene inside helium droplets.

TABLE 1: Comparison of REMPI and HENDI Line Positions (cm^{-1}), Shifts (cm^{-1}), Intensities (Relative to the Strongest Peak), and Vibronic Assignments for the S_1−S_0 Transition of Biphenylene

HENDI	REMPI[27]	shift	rel. int.	assignment
25 691.5			8.8	ν_{39} (b_{2u})
25 726.3			30.0	ν_{38} (b_{2u})
26 131.8			30.4	ν_{36} (b_{2u})
26 161.6	26 180	−18.4	100.0	ν_{35} (b_{2u})
26 460.5			9.3	
26 476.8			13.2	ν_{38} (b_{2u}) + ν_9 (a_g)
26 538.1			20.3	ν_{38} (b_{2u}) + 2 ν_{10} (a_g)
26 566.6	26 583	−16.4	89.2	ν_{35} (b_{2u}) + ν_{10} (a_g)
26 862.1			10.8	ν_{38} (b_{2u}) + ν_7 (a_g)
26 867.8			12.0	
26 882.2			13.4	ν_{36} (b_{2u}) + ν_9 (a_g)
26 894.1			21.9	?
26 911.9	26 929	−17.1	36.8	ν_{35} (b_{2u}) + ν_9 (a_g)
26 937.2			8.3	
26 941.1			9.0	ν_{36} (b_{2u}) + 2 ν_{10} (a_g)
26 970.6	26 986	−15.4	26.1	ν_{35} (b_{2u}) + 2 ν_{10} (a_g)
27 199.0			7.5	
27 214.5			8.0	
27 293.4	27 309	−15.6	37.1	ν_{35} (b_{2u}) + ν_7 (a_g)
27 301.5			23.6	?
27 317.0			20.1	ν_{35} (b_{2u}) + ν_{10} (a_g) + ν_9 (a_g)
27 321.8			11.3	
27 345.1			8.0	ν_{36} (b_{2u}) + 3 ν_{10} (a_g)
27 373.5	27 389	−15.5	10.7	ν_{35} (b_{2u}) + 3 ν_{10} (a_g)
27 620.5			11.6	

transitions was calculated at the TD-B3LYP level. The Gaussian03 package was used to carry out the calculations.[36]

3. Results

Monomer

The HENDI S_1−S_0 spectrum of BP, presented in Figure 1, is similar to previously reported REMPI spectra. The peaks around 25 750 cm^{-1} were previously assigned to hot band transitions by Zimmermann.[27] The occurrence of these peaks in HENDI spectrum rules out the hot band assignment because at the temperature of the droplets there are no thermally populated excited vibrational states.

The list of peak positions, assignments and comparisons to explicitly tabulated REMPI peaks, is presented in Table 1. The shifts from the gas-phase positions are similar (∼−16 cm^{-1}) for different vibronic bands, which all involve excitations of a_g modes built upon a false origin of mode ν_{35} (b_{2u}).

Although the theory for Herzberg−Teller allowed transitions is well established,[37] practical calculations have been limited

to a couple of molecules. A computer code, HOTFCHT, has been developed to calculate Franck−Condon and Herzberg−Teller integrals.[38] This code has been applied to spectra of benzene and pyrazine,[38] anthracene, pentacene, pyrene, octatetraene, and styrene.[39] Alternatively, cumbersome calculations involving polynomial expansion of electronic transition dipole moments along normal modes have been carried out for benzene, formaldehyde, acetone, and formic acid.[40] Instead, a simplified approximation is preferred here to calculate the intensity distribution.

The intensity of an electric dipole absorption transition between two vibronic states $|\kappa(\vec{q},\vec{Q})\rangle$ and $|\mu(\vec{q},\vec{Q})\rangle$ is proportional to the product of the transition frequency and the square of the transition electric dipole moment. The transition dipole moment can be written as

$$\vec{M}_{\kappa\mu} \approx \langle\chi_{k,\kappa}(\vec{Q})|\langle\psi_k(\vec{q},\vec{Q})|\vec{M}(\vec{q},\vec{Q})|\psi_m(\vec{q},\vec{Q})\rangle|\chi_{m,\mu}(\vec{Q})\rangle = \\ \langle\chi_{k,\kappa}(\vec{Q})|\vec{M}_{km}(\vec{Q})|\chi_{m,\mu}(\vec{Q})\rangle \quad (1)$$

where $|\psi_k(\vec{q},\vec{Q})\rangle$ or $|\psi_m(\vec{q},\vec{Q})\rangle$ and $|\chi_{k,\kappa}(\vec{Q})\rangle$ or $|\chi_{m,\mu}(\vec{Q})\rangle$ are the final (k,κ) and initial (m,μ) electronic and vibrational states respectively. $\vec{M}_{km}(\vec{Q})$ is the electronic transition dipole moment, and $\vec{q}$ and $\vec{Q}$ represent the electronic and nuclear coordinates.

The electronic transition dipole moment can be expressed as a Taylor expansion around the equilibrium position

$$\vec{M}_{km}(\vec{Q}) \approx \vec{M}_{km}(\vec{Q}_0) + \sum_{\eta=1}^{N}\left(\frac{\partial\vec{M}_{km}(\vec{Q})}{\partial Q_\eta}\right)_{\vec{Q}_0}(Q_\eta - Q_\eta^0) + \dots \quad (2)$$

where N is the number of vibrational degrees of freedom. Truncation at the first term yields the Franck−Condon approximation

$$\vec{M}_{\kappa m} \approx \vec{M}_{km}(\vec{Q}_0)\langle\chi_{k,\kappa}(\vec{Q})|\chi_{m,\mu}(\vec{Q})\rangle \quad (3)$$

which ignores the dependence of electronic transition dipole on nuclear coordinates. Because eq 3 is zero for the forbidden S_1-S_0 transition of BP, the second term is used to calculate the intensities.

$$\vec{M}_{\kappa\mu}(\vec{Q}) \approx \left\langle\chi_{k,\kappa}(\vec{Q})\left|\sum_{\eta=1}^{N}\left(\frac{\partial\vec{M}_{km}(\vec{Q})}{\partial Q_\eta}\right)_{\vec{Q}_0}(Q_\eta - Q_\eta^0)\right|\chi_{m,\mu}(\vec{Q})\right\rangle \quad (4)$$

$$\vec{M}_{\kappa\mu}(\vec{Q}) \approx \sum_{\eta=1}^{N}\left(\frac{\partial\vec{M}_{km}(\vec{Q})}{\partial Q_\eta}\right)_{\vec{Q}_0}\langle\chi_{k,\kappa}(\vec{Q})|(Q_\eta - Q_\eta^0)|\chi_{m,\mu}(\vec{Q})\rangle \quad (5)$$

The derivative of the electronic transition dipole moment is estimated by TD−DFT/6-31G calculations at slightly displaced nuclear coordinates for each b_{2u} mode. The result of the calculation is rescaled by the factor used for displacing the nuclear coordinates, typically 1%. The integral in eq 5 is estimated using the properties of ladder operators of N-dimensional harmonic oscillator:

$$\langle\vec{v}'|\hat{Q}_\eta|\vec{v}\rangle = \sqrt{\frac{\hbar}{2\omega_\eta}}[\sqrt{v_n}\langle\vec{v}'|v_1,\dots v_\eta - 1,\dots,v_N\rangle + \\ \sqrt{v_n+1}\langle\vec{v}'|v_1,\dots v_\eta + 1,\dots,v_N\rangle] \quad (6)$$

which converts Herzberg−Teller integrals into a sum of Franck−Condon integrals of the type $<1|1>$. Since only the
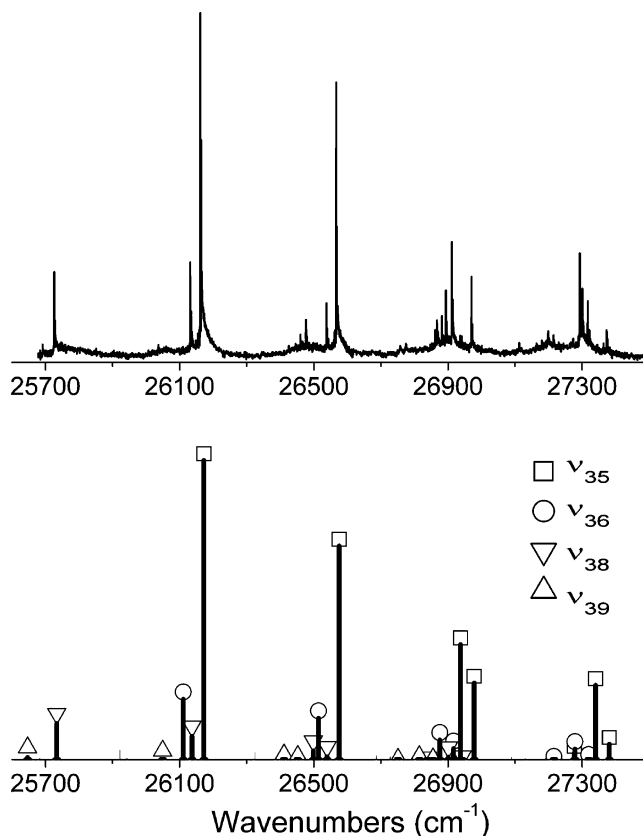

Figure 2. Experimental and calculated spectral intensity of the Biphenylene S_1-S_0 transition.

ground vibrational states of the ground electronic state are involved in the transition, only the second term of the sum is nonzero. The Franck−Condon integrals are evaluated using the MolFC code kindly provided by Dr. Borrelli.[41] The product of the derivatives and Herzberg−Teller integrals are divided by the square root of the reduced mass of each mode, as provided by the Gaussian code, thus finally reaching units of dipole. The intensity distribution for the a_g mode progressions starting at each false origin is calculated with the MolFC program.

A comparison of the observed S_1-S_0 spectra with the calculated relative intensities is presented in Figure 2. The wavenumber of the excited-state b_{2u} vibrational modes are scaled so that ν_{35} matches the experimental value. For the a_g modes of the electronic excited state, experimental values are used. The agreement is very good even though higher order terms of the Taylor expansion and anharmonic effects are neglected. The feature assigned as a hot band by Zimmerman is a false origin built on mode 38.

A comparison of the normalized b_{2u} intensities with the previous calculation[28] together with graphical representation of the normal modes is presented in Table 2. The geometry change induced by the first two modes is similar to the change due to the electronic excitation, shortening of the benzene−benzene distance and elongation of the benzene moieties along the short axis. The frequencies of the modes in the S_1 state are calculated at the RCIS level and scaled to match the experimentally known values.

Dimers. Increasing the pick-up cell pressure causes multiple pickups by the droplets and consequent clustering. BP clusters, mostly dimers judged by the pressure range at which the measurements were carried out, show up as broad peaks to the red of the main sharp peaks. The broad peak to the red of the most intense false origin has a shift of -116 cm^{-1} and a fwhm

Biphenylene Inside Helium Nanodroplets

J. Phys. Chem. A, Vol. 111, No. 31, 2007 **7627**

TABLE 2: Relative Intensities of Herzberg–Teller Transition Origins

b_{2u}	Calc.[a]	Exp.[b]	Exp. Inten.[c]	Calc. Inten.[d]	Calc. Inten.[e]	Mode
ν_{35}	1622	1612	1.00	1.00	1.00	
ν_{36}	1561	1582	0.25	0.22	0.12	
ν_{37}	1372			0.03	0.00	
ν_{38}	1184	1176	0.22	0.15	0.01	
ν_{39}	1096	1141	0.04	0.04	0.01	
ν_{40}	730			0.00	0.05	
ν_{41}	225			0.01	0.01	

[a] Calculated S_0 frequencies scaled to ν_{35} frequency of 1622 cm^{-1}, as reported by Zimmermann, in cm^{-1}. [b] Experimental $S_1 \leftarrow S_0$ excess term value over Zimmerman's estimated origin of 24 550 cm^{-1}, in cm^{-1}. [c] Experimental intensity normalized to ν_{35}. [d] Calculated intensity normalized to ν_{35}. [e] From ref 28, calculated intensity normalized to ν_{35}.
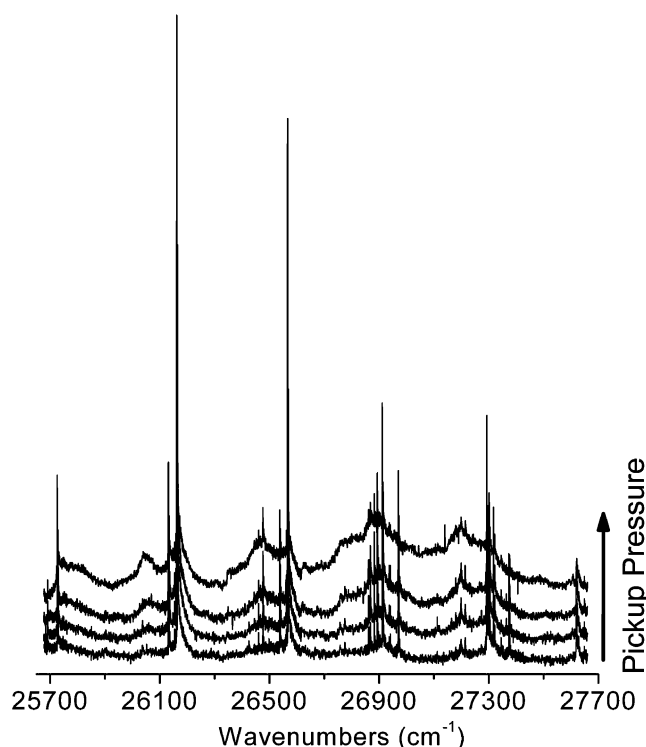
Figure 3. Spectra of Biphenylene inside helium droplets with increasing pick-up pressure.

of 56 cm^{-1}. These numbers are close to the experimentally determined values for naphthalene dimers[42] (shift, -137 cm^{-1} and fwhm, 128 cm^{-1}) and to a lesser extent, anthracene dimers[43] (shift, -507 cm^{-1} and fwhm, 190 cm^{-1}). The smaller shift and narrower peak width could be attributed to the large geometrical change of BP, which would reduce the interaction of the dimers in the sandwich configuration. The absence of sharp dimer peaks in the spectrum argues against a T-shaped geometry.[44]

ZPL and Phonon Wings. The blow up of several monomer vibronic peaks, Figure 4, shows two sharp zero phonon lines separated by 2.4 cm^{-1} with intensity ratio of 3:2 and fwhm of
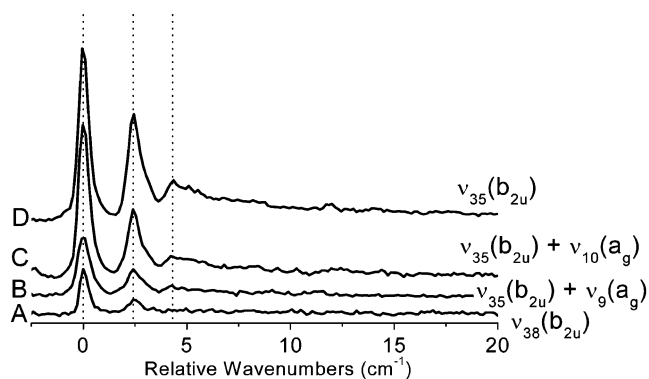
Figure 4. Expanded view of Biphenylene vibronic transitions with absolute band center positions (cm^{-1}): A, 25726.3; B, 26911.8; C, 26566.6; and D, 26161.7.
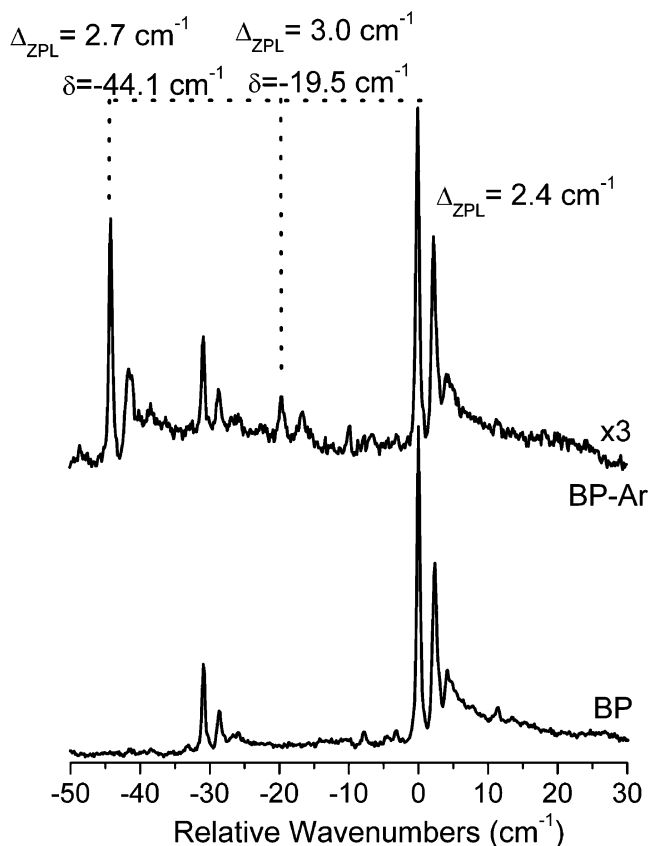
Figure 5. Spectra of Biphenylene and Biphenylene−Ar complex around ν_{35} false origin.

0.7 and 0.9 cm^{-1}, respectively, regardless of the excess vibrational quanta. The phonon wing following the peak to the high-energy side has a maximum at 4.3 cm^{-1} relative to the first ZPL and it extends about 30 cm^{-1} to the blue. Although the shape of the phonon wing is similar to previous observations,[11] the amount of ZPL splitting is one of the largest values yet reported. For tetracene,[8] there are 2 ZPLs split by 1.1 cm^{-1}, whereas for indole and 3-methyl indole,[45] there are 3 ZPLs each split by about 2.0 cm^{-1}.

Van der Waals Complexes. The van der Waals complexes are created inside the droplets by consecutive pickup of BP from the oven and argon or oxygen from the gas pickup cell. The spectrum of BP-argon complex near the false origin ν_{35} is presented in Figure 5. Two different peak groups are assigned to the complex: the more intense doublet at -44.1 cm^{-1} and the weaker doublet at -19.5 cm^{-1} relative to the false origin.

Both of these peaks belong to the 1:1 complex because their intensity changes at the same rate with argon pickup pressure. It must be emphasized that the splitting of the ZPL is retained for both complexes unlike for the dominant tetracene-argon complex inside helium nanodroplets.[8,9] For the more intense complex peaks, the ZPL splitting increases from 2.4 to 2.7 cm^{-1}. The stronger of the ZPLs preserves its width (fwhm 0.5 cm^{-1}), whereas the weaker ZPL is slightly broadened (fwhm 1.2 cm^{-1}). On the other hand, for the weaker complex peaks, the splitting increases to 3.0 cm^{-1} and both ZPLs are slightly broadened (fwhm 0.95 and 1.25 cm^{-1}). The weaker doublet is blue-shifted from the more intense complex peak by about 25 cm^{-1}. Although our calculations indicate that the frequency of argon out-of-plane vibration is about 16 cm^{-1} (using the potential energy surface presented in the discussion section), we cannot definitively assign this weak feature as such, because this type of vibrations were not observed in tetracene-argon complex inside helium droplets which was attributed as due to a damping effect of the droplet.[8]

It is perhaps useful to compare our results on the Ar-biphenyl complex with those previously obtained for the Ar-tetracene complex.[46] There, two sets of peaks were also observed, a stronger one with a red shift of −38.4 cm^{-1}, and a much weaker pair of peaks with a shift of the stronger component of −9.2 cm^{-1}, which are less than we have observed for BP (−44.1 and −19.4 cm^{-1} shifts respectively). In the tetracene case, the stronger Ar complex has the ∼1 cm^{-1} ZPL splitting completely suppressed, for the less shifted case the ZPL splitting increased to ∼3.4 cm^{-1}. In the BP case, the features due to both BP complexes have an increase in the ZPL splitting, the first molecule for which we are aware of this happening. In the tetracene case, the authors assigned the less shifted peaks as due to binding of Ar in the plane of the aromatic molecule, largely based on both the reduced shift and the retention (in fact, augmentation) of the ZPL splitting. Given that the binding of Ar to BP also produces two solvation features, both of which retrain the ZPL splitting, the prior assignment appears to be less certain. The upper (and stronger) ZPL of tetracene contained a very small residual splitting that was retained in both of the Ar complexes; unfortunately, our spectral resolution is not sufficient to have been able to observe this, if present, in the BP spectra.

The spectrum of BP-oxygen complex near the false origin ν_{35} is presented in Figure 6. Oxygen was selected for study as it is possible for O_2 to induce rapid intersystem crossing, as was exploited by Parmenter.[47] It was previously pointed out that the resulting reduced quantum yield for emission could be observed in depletion spectroscopy as enhanced signals for spectral features of O_2 complexes.[18] The broad peak at −64.7 cm^{-1} relative to the false origin is identified as the oxygen complex. Although a resolved splitting is not observed, the asymmetry of the broadened peak (fwhm∼7.0 cm^{-1}) is consistent with convolution of the split ZPLs observed in BP with a broadening in the BP−O_2 species. Due to limited time, we have not attempted to observe complexes of BP with other gases, though it would be relatively straightforward to do so.

4. Discussion

In order to explain the peak shapes of BP and its van der Waals complexes, it is desirable to have potential energy surfaces describing the interactions. Since we know of no *ab inito* potential for BP-rare gas pairs, we chose to approximate the interaction by extending results of benzene−rare gas pairs. We have chosen the angle dependent Lennard-Jones potential
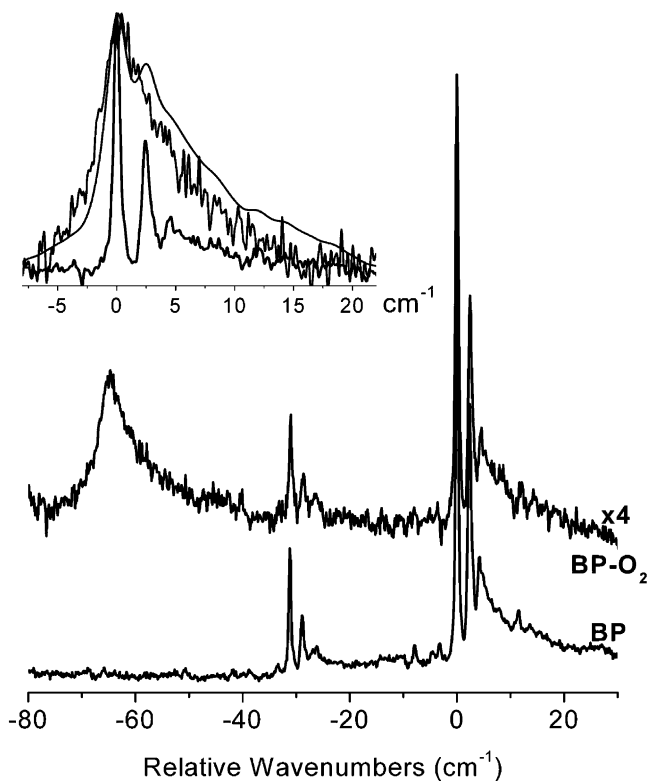

Figure 6. Spectra of Biphenylene and Biphenylene−O_2 complex around ν_{35} false origin. (Inset) Asymmetric complex peak, the monomer peak, and the monomer peak convoluted with a Lorentzian (fwhm: 2.08 cm^{-1}) are overlapped.

(6−12 for H−He; 8−14-θ for C−He), which was used by the Whaley group[48] to fit Hobza et al. 's MP2 level benzene-helium potential calculation.[49] This potential predicts global minima of −66.0 cm^{-1} above the center of the benzene the ring at an equilibrium distance of 3.27 Å. We scaled the parameters of this potential to match the most recent CCSD(T) calculation, which places the global minima of D_e= −89.6 cm^{-1} at 3.16 Å above the center of the ring.[50]

The form of the analytical fit is given in eqs 7−9. The new parameters are ϵ_{C-He}=14.54 cm^{-1}, ϵ_{H-He}=18.25 cm^{-1}, σ_{C-He}= 3.51 Å and σ_{H-He}=2.63 Å.

$$E_{C-He}(\vec{r}) = 4\epsilon_{C-He}\cos^2\theta\left[\left(\frac{\sigma_{C-He}\cos\theta}{|\vec{r}|}\right)^{14} - \left(\frac{\sigma_{C-He}\cos\theta}{|\vec{r}|}\right)^{8}\right] \quad (7)$$

$$E_{H-He}(\vec{r}) = 4\epsilon_{H-He}\left[\left(\frac{\sigma_{H-He}}{|\vec{r}|}\right)^{12} - \left(\frac{\sigma_{H-He}}{|\vec{r}|}\right)^{6}\right] \quad (8)$$

$$E_{benzene-He}(\vec{r}) = \sum_i E_{C-He}(\vec{r} - \vec{r}_i) + \sum_j E_{H-He}(\vec{r} - \vec{r}_j) \quad (9)$$

where θ is defined as the angle between the vector $(\vec{r} - \vec{r}_n)$ and the vector perpendicular to the molecular surface. For selected points, the values for the modified Lennard-Jones potential and CCSD(T) calculation are compared in Table 3. The lack of an azimuthal dependence to the He-atom interactions may be responsible for the relatively poor prediction of the energy of the first saddle point. Although the overall agreement is modest, the modified potential is used to model the BP−helium interaction. It is noted, however, that for BP, the four carbon atoms that make up the four member ring have different bond

Biphenylene Inside Helium Nanodroplets

J. Phys. Chem. A, Vol. 111, No. 31, 2007 **7629**

TABLE 3: Benzene−Helium Interaction Energies (cm⁻¹) at Given Positions (Å)

	position $(x; y; z)^a$	E (fit)	position $(x; y; z)^a$	E (CCSD(T))[50]
minima	0.0; 0.0; 3.16	−89.58	0.0; 0.0; 3.16	−89.59
	4.82; 0.0; 0.0	−38.73	4.74; 0.0; 0.0	−44.73
saddle points	2.81; 0.0; 2.62	−59.18	2.93; 0.0; 3.24	−28.87
	0.0; 5.40; 0.0	−23.07	0.0; 5.39; 0.0	−20.76

^{a} x-axis intersects C−C bonds, y-axis overlaps with C atoms, and z-axis is the 6-fold symmetry axis.

TABLE 4: Benzene−Argon Interaction Energies (cm⁻¹) at Given Positions (Å)

	position $(x; y; z)^a$	E (fit)	position $(x; y; z)^a$	E (CCSD(T))[51]
minima	0.0; 0.0; 3.55	−388.31	0.0; 0.0; 3.56	−386.97
	5.10; 0.0; 0.0	−163.93	5.03; 0.0; 0.0	−216.97
saddle points	2.96; 0.0; 2.88	−254.36	3.42; 0.0; 3.02	−203.17
	0.0; 5.65; 0.0	−101.31	0.0; 5.52; 0.0	−123.17

^{a} x-axis intersects C−C bonds, y-axis overlaps with C atoms, and z-axis is the 6-fold symmetry axis.
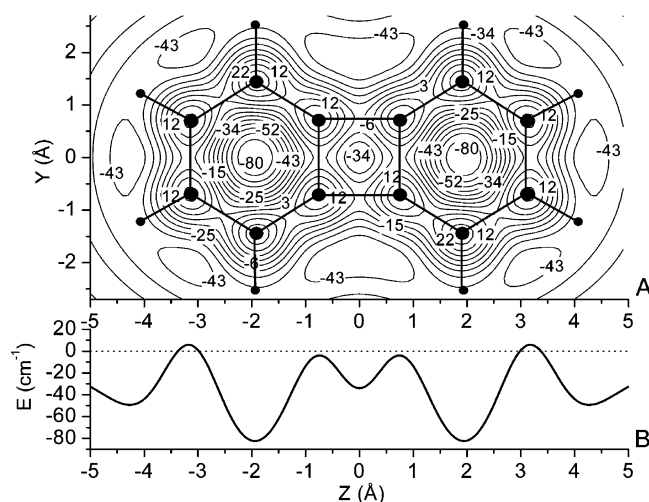

Figure 7. (A) Biphenylene-helium interaction surface calculated at X (height above molecular plane) = 3.21 Å. (B) Potential energy at Y = 0.0 Å and X = 3.21 Å.

angles and partners than the carbon atoms of benzene, and thus transferability of the potential parameters is less reliable for those parts of the potential where binding to these carbons are most important.

The same formalism was followed to generate the benzene−argon potential. The parameters of the benzene-helium interaction were scaled to match the CCSD(T) calculation for benzene−argon interaction.[51] The parameters used are ϵ_{C-Ar} = 60.59 cm⁻¹, ϵ_{H-Ar} = 76.05 cm⁻¹, σ_{C-Ar} = 3.81 Å, and σ_{H-Ar} = 2.86 Å. A comparison of the modified Lennard-Jones potential and the CCSD(T) calculation are given for selected points in Table 4.

Equipped with a BP−helium potential, one can, now, attempt to explain the ZPL and phonon wing structures of the spectra. The Lennard-Jones potential of BP−helium pair, Figure 7, predicts two different minima positions over the molecular plane. Although one of them is located over either of the benzene rings at R_e = 3.21 Å with a depth of D_e = −82.4 cm⁻¹, the second one is located over the 4-member ring at R_e = 3.51 Å with D_e = −62.6 cm⁻¹. Clearly these two locations cannot be occupied at the same time since the He−He distance would be 1.95 Å. The He−He pair potential of Aziz[52] places the minimum at R_e

= 2.96 Å and D_e = −7.68 cm⁻¹. Furthermore, employing the Numerov-Cooley method,[53] we could not find a bound state for a helium atom in the potential well over the 4-member ring. On the other hand, two helium atoms can be simultaneously localized over both of the 6-member rings, because the separation in this case is 3.85 Å. In this model, the 4 equivalent global minima positions can be simultaneously occupied by helium atoms appearing to leave out the possibility for different isomers or tunneling as proposed for explaining the ZPL splitting of tetracene in helium droplets.[9]

In the case of BP−Ar system, the more intense complex peak shifted by −44.1 cm⁻¹ from the false origin is most probably the complex with argon localized over one of the benzene rings. The weaker complex peak at −19.5 cm⁻¹ can be assigned to the complex with argon atom localized over the 4-member ring. The retaining of the ZPL splitting after complexation with argon cannot be explained with the current understanding of the source of the splitting. Although the complexation disturbs the first solvation shell, the splitting remains almost the same.

The oxygen complex has only one structural isomer, most probably with oxygen localized over one of the benzene rings. However, when oxygen binds to the surface on the bond side, its relative orientation with respect to the ring will give rise to slightly different potential energy surfaces. The broadening of the peak could be the result of these multiple "local" isomers, which smear out the splitting. Alternatively, oxygen can be speeding up intersystem crossing or perhaps vibrational relaxation.

Because the splitting is observed with argon complexes and that the same splitting could be retained by the oxygen complex but is lost in the broadening, one has to consider whether the transition is split for the isolated molecule. The only high-resolution jet spectrum up to date does not present any close up structure for peaks, but it does not mention any anomalous splitting either.

5. Conclusion

We have recorded the S_1-S_0 transition of BP inside helium nanodroplets by depletion method. The spectrum is similar to the jet spectrum recorded with REMPI technique. We established that the previous hot band assignments are not correct. A simplified Herzberg−Teller analysis for the peak intensities is sufficient to identify the active normal modes of this transition. However, the behavior of this molecule inside helium nanodroplets is quite different than the other molecules studied to date. The ZPL splitting is larger than that of other molecules studied to date. The splitting is retained in case of Ar complexation despite the expected substantial change in helium solvation given that one of the most favorable helium binding sites will be displaced. This observation is difficult to explain with the current understanding that the splitting arises due to the interaction of helium atoms, primarily from the first solvation shell, and the molecule.

Our calculations suggest that there is significant electron density change over the molecular plane due to S_1-S_0 transition, however it is difficult to predict how the helium environment would response to it. It would be important to obtain accurate *ab initio* potential energy surfaces describing the interaction of helium and BP both in the S_0 and S_1 states.

practitioner of the art of molecular beam infrared spectroscopy. His clean experimental style will remain a standard against which the quality of molecular beam experiments will be measured for a long time. We will sorely miss not only his science but also his ironic, heart-warming smile, and, above all, his unconditional friendship.

References and Notes

(1) Stienkemeier, F.; Vilesov, A. F. *J. Chem. Phys.* **2001**, *115*, 10119.

(2) Toennies, J. P.; Vilesov, A. F. *Angew. Chem., Int. Ed.* **2004**, *43*, 2622.

(3) Stienkemeier, F.; Lehmann, K. K. *J. Phys. B: At., Mol. Opt. Phys.* **2006**, *39*, R127.

(4) Schmied, R.; Çarçabal, P.; Dokter, A. M.; Lonij, V. P. A.; Lehmann, K. K.; Scoles, G. *J. Chem. Phys.* **2004**, *121*, 2701.

(5) Boatwright, A.; Besley, N. A.; Curtis, S.; Wright, R. R.; Stace, A. J. *J. Chem. Phys.* **2005**, *123*, 021102.

(6) Lindinger, A. Ph.D. Thesis, Georg-August-Universitaet, Gottingen, 1998.

(7) Krasnokutski, S.; Rouille, G.; Huisken, F. *Chem. Phys. Lett.* **2005**, *406*, 386.

(8) Hartmann, M.; Lindinger, A.; Toennies, J. P.; Vilesov, A. F. *Chem. Phys.* **1998**, *239*, 139.

(9) Hartmann, M.; Lindinger, A.; Toennies, J. P.; Vilesov, A. F. *J. Phys. Chem. A* **2001**, *105*, 6369.

(10) Lindinger, A.; Toennies, J. P.; Vilesov, A. F. *Phys. Chem. Chem. Phys.* **2001**, *3*, 2581.

(11) Hartmann, M.; Lindinger, A.; Toennies, J. P.; Vilesov, A. F. *Phys. Chem. Chem. Phys.* **2002**, *4*, 4839.

(12) Lehnig, R.; Slenczka, A. *J. Chem. Phys.* **2005**, *122*, 244317.

(13) Wewer, M.; Stienkemeier, F. *J. Chem. Phys.* **2003**, *120*, 1239.

(14) Wewer, M.; Stienkemeier, F. *Phys. Rev. B.* **2003**, *67*, 125201.

(15) Lehnig, R.; Slenczka, A. *J. Chem. Phys.* **2003**, *118*, 8256.

(16) Lehnig, R.; Slenczka, A. *J. Chem. Phys.* **2004**, *120*, 5064.

(17) Lehnig, R.; Slenczka, A. *ChemPhysChem* **2004**, *5*, 1014.

(18) Çarçabal, P.; Schmied, R.; Lehmann, K. K.; Scoles, G. *J. Chem. Phys.* **2004**, *120*, 6792.

(19) Staicu, A.; Krasnokutski, S.; Rouille, G.; Henning, T.; Huisken, F. *J. Mol. Struct.* **2006**, *786*, 105.

(20) Rouille, G.; Krasnokutski, S.; Huisken, F.; Henning, T.; Sukhorukov, O.; Staicu, A. *J. Chem. Phys.* **2004**, *120*, 6028.

(21) Hartmann, M.; Mielke, F.; Toennies, J. P.; Vilesov, A. F.; Benedek, G. *Phys. Rev. Lett.* **1996**, *76*, 4560.

(22) Schmied, R. Ph.D. Thesis, Princeton University, Princeton, 2006.

(23) Zanon, I. *J. Chem. Soc. Faraday Trans. 2* **1973**, *69*, 1164.

(24) Nickel, B.; Hertzberg, J. *Chem. Phys.* **1989**, *132*, 219.

(25) Hertzberg, J.; Nickel, B. *Chem. Phys.* **1989**, *132*, 235.

(26) Elsaesser, T.; Larmer, F.; Kaiser, W.; Dick, B.; Niemeyer, M.; Luttke, W. *Chem. Phys.* **1988**, *126*, 405.

(27) Zimmermann, R. *A. I. P. Conf. Proc.* **1996**, *388*, 399.

(28) Marconi, G. *Chem. Phys. Lett.* **1990**, *169*, 617.

(29) Callegari, C.; Lehmann, K. K.; Schmied, R.; Scoles, G. *J. Chem. Phys.* **2001**, *115*, 10090.

(30) Knuth, E. L.; Schilling, B.; Toennies, J. P. In *19th International Symposium on Rarefied Gas Dynamics*; Harvey, J., Lord, G., Eds.; Oxford University Press Inc.: Oxford, 1994; Vol 19, pp 270−275.

(31) Infrared Laboratories: Tucson, AZ.

(32) Positive Light, Inc.: Los Gatos, CA.

(33) Littman, M. G. *Opt. Lett.* **1978**, *3*, 138.

(34) EXFO Burleigh Products Group, Inc.: Victor, NY.

(35) National Instruments Corp.: Austin, TX.

(36) Frisch, M. J.; Trucks, G. W.; Schlegel, H. B.; Scuseria, G. E.; Robb, M. A.; Cheeseman, J. R.; Montgomery, J. A., Jr.; Vreven, T.; Kudin, K. N.; Burant, J. C.; Millam, J. M.; Iyengar, S. S.; Tomasi, J.; Barone, V.; Mennucci, B.; Cossi, M.; Scalmani, G.; Rega, N.; Petersson, G. A.; Nakatsuji, H.; Hada, M.; Ehara, M.; Toyota, K.; Fukuda, R.; Hasegawa, J.; Ishida, M.; Nakajima, T.; Honda, Y.; Kitao, O.; Nakai, H.; Klene, M.; Li, X.; Knox, J. E.; Hratchian, H. P.; Cross, J. B.; Bakken, V.; Adamo, C.; Jaramillo, J.; Gomperts, R.; Stratmann, R. E.; Yazyev, O.; Austin, A. J.; Cammi, R.; Pomelli, C.; Ochterski, J. W.; Ayala, P. Y.; Morokuma, K.; Voth, G. A.; Salvador, P.; Dannenberg, J. J.; Zakrzewski, V. G.; Dapprich, S.; Daniels, A. D.; Strain, M. C.; Farkas, O.; Malick, D. K.; Rabuck, A. D.; Raghavachari, K.; Foresman, J. B.; Ortiz, J. V.; Cui, Q.; Baboul, A. G.; Clifford, S.; Cioslowski, J.; Stefanov, B. B.; Liu, G.; Liashenko, A.; Piskorz, P.; Komaromi, I.; Martin, R. L.; Fox, D. J.; Keith, T.; Al-Laham, M. A.; Peng, C. Y.; Nanayakkara, A.; Challacombe, M.; Gill, P. M. W.; Johnson, B.; Chen, W.; Wong, M. W.; Gonzalez, C.; Pople, J. A. *Gaussian 03*, revision C.02; Gaussian, Inc.: Wallingford, CT, 2004.

(37) Herzberg, G.; Teller, E. *Z. Phys. Chem. B.* **1933**, *21*, 410.

(38) Berger, R.; Fischer, C.; Klessinger, M. *J. Phys. Chem. A* **1998**, *102*, 7157.

(39) Dierksen, M.; Grimme, S. *J. Chem. Phys.* **2004**, *120*, 3544.

(40) Borges, I.; Rocha, A. B.; Bielschowsky, C. E. *Braz. J. Phys.* **2005**, *35*, 971.

(41) Borrelli, R.; Peluso, A. *MolFC: A program for Franck-Condon Integrals Calculation*; Salerno University: Salerno, Italy, 2004; available at http://pcdual.chem.unisa.it

(42) Wessel, J. E.; Syage, J. A. *J. Phys. Chem.* **1990**, *94*, 737.

(43) Piuzzi, F.; Dimicoli, I.; Mons, M.; Millie, P.; Brenner, V.; Zhao, Q.; Soep, B.; Tramer, A. *Chem. Phys.* **2002**, *275*, 123.

(44) Das, A.; Mahato, K. K.; Chakraborty, T. *J. Chem. Phys.* **2001**, *114*, 8310.

(45) Lindinger, A.; Lugovoj, E.; Toennies, J. P.; Vilesov, A. F. *Z. Phys. Chem.* **2001**, *215*, 401.

(46) Portner, N.; Vilesov, A. F.; Havenith, M. *Chem. Phys. Lett.* **2001**, *343*, 281.

(47) Parmenter, C. S. *J. Phys. Chem.* **1982**, *86*, 1735.

(48) Kwon, Y.; Whaley, K. B. *J. Chem. Phys.* **2001**, *114*, 3163.

(49) Hobza, P.; Bludsky, O.; Selzle, H. L.; Schlag, E. W. *J. Chem. Phys.* **1992**, *97*, 335.

(50) Lee, S.; Chung, J. S.; Felker, P. M.; Cacheiro, J. L.; Fernandez, B.; Pedersen, T. B.; Koch, H. *J. Chem. Phys.* **2003**, *119*, 12956.

(51) Koch, H.; Fernandez, B.; Makarewicz, J. *J. Chem. Phys.* **1999**, *111*, 198.

(52) Janzen, A. R.; Aziz, R. A. *J. Chem. Phys.* **1997**, *107*, 914.

(53) Cooley, J. W. *Math. Comp.* **1961**, *15*, 363.